Time-space distribution of long-range atmospheric predictability

Thomas Reichler and John O. Roads

Scripps Institution of Oceanography

University of California San Diego, 9500 Gilman Dr., La Jolla, CA 92093-0224,

Correspondence to: John O. Roads (jroads@ucsd.edu)

Friday, May 30, 2003

Table of Contents

Abstract

The global 3-dimensional structure of long-range (2 weeks to 1 season) atmospheric predictability was investigated with a general circulation model. The main focus was to ascertain the role of atmospheric initial conditions for such predictability as a function of lead time and space. Four types of predictability experiments with different types of initial and boundary conditions were conducted to this end. The experiments were verified against reanalysis and model data to determine real forecast skill as well as skill under the perfect model assumption. Spatial maps and vertical cross sections of predictability at different lead times and for the two contrasting seasons were analyzed to document the varying influence of initial and boundary conditions on predictability. It was found that the atmosphere was remarkably sensitive to initial conditions on the week 3-6 forecast range. Particularly, the troposphere over Antarctica, the region over the tropical Indian Ocean, and the lower stratosphere were affected. It was shown that most of the initial condition memory was related to the persistent nature of the atmosphere in these regions, which in turn was linked to the major modes of atmospheric variability.

1. Introduction

Three fundamental sources affect dynamical atmospheric predictability: the model, which contains the physical principles that govern atmospheric flow, the initial atmospheric state, and the atmospheric boundary conditions during the forecast. Predictability is limited because none of these are perfect. Small unavoidable errors grow rapidly through non-linear interactions. Classical studies of predictability were mostly concerned with the effect of initial conditions on predictability, and determined its loss due to the growth of initial errors in a chaotic atmosphere. The associated limit in forecasting the instantaneous atmospheric state (or weather) was established with simplified models to be about 2-3 weeks (e.g., Lorenz, 1969; Lorenz, 1982). Although chaotic, the atmosphere can be forced externally by its boundaries towards a particular climate state. This boundary forced predictability effect offers the potential for predictability on longer time scales, which has been the focus of more recent studies of predictability. In particular, sea surface temperature (SST) variations associated with the El Niño Southern Oscillation (ENSO) phenomenon have significant impacts on long-range predictability.

The current study addresses the question whether initial conditions can affect predictability beyond the classical limit. In particular, this study is focused on the long-range or sub-seasonal time scale, which includes everything from 2 weeks to about 3 months. Since this time scale represents a mixture between the weather and climate and prediction problem, it is likely that both initial and boundary conditions are important. This has recently been demonstrated by Reichler and Roads (2003) (hereafter RR), who showed that initial conditions dominated a forecast during the first four weeks, and that even thereafter initial conditions contributed to improved predictability. There are certainly

several physical mechanisms that might contribute to long-range predictability from initial conditions, associated with long-lived persistent and periodic phenomena. One example is the intraseasonal oscillation (Madden and Julian, 1972), which is established through a certain combination of atmospheric initial and ocean boundary conditions. There are other examples of how initial conditions might affect long-range predictability, like blocking events, or slow shifts of major modes. Recently, observational evidence suggested that the downward propagation of long-lived stratospheric anomalies into the troposphere might have implications for long-range predictability (Thompson et al., 2002).

Since predictability is in general a function of space, season, and lead time, we investigated globally the full 3-dimensional structure of predictability of geopotential heights, and examined how it changed with lead time, season, and strength of the boundary forcing. As we will show, there exists considerable initial condition produced predictability at the week 3-6 time range. This prompted further analysis, aimed at finding possible physical mechanisms behind the large sensitivity to initial conditions. In particular, we investigated how this effect was related to atmospheric persistence and low-frequency variability associated with major atmospheric modes.

Understanding the role of atmospheric initial conditions is important for progress in the long-term predictability effort. It is, for example, still an open question as to just how sensitive the atmosphere is to initial conditions, and when and where initial conditions can be important for long-range predictability. For operational seasonal forecasts, for example, the various centers use different initialization strategies. At the International Research Institute for Climate Predictions (IRI) a previous forecast rather than analysis are used to initialize the atmospheric model (see Mason et al., 1999). However, at the National Centers

for Environmental Prediction (NCEP) (Kanamitsu et al., 2002), and at the Scripps Experimental Climate Prediction Center (ECPC) (Roads et al., 2001) the initial conditions used for weather predictions (analysis) are also used for seasonal forecast models.

We used a model-based approach and developed four basic types of predictability experiments. Each experiment was forced with different types of initial and boundary conditions, so that we were able to determine their individual contribution to predictability. In most cases, the experiments were verified under the so called perfect model assumption, which compares the forecasts against simulations with the same model. This way we avoided complications with model related errors and, as will be discussed later, could reduce substantially the sampling problem. However, since we were also curious as to whether our idealized findings were still applicable in the real world, we also compared the experiments against real world observations.

The paper is structured as follows: In Section 2, model, data and analysis method are described. Section 3 presents a 3-dimensional analysis of monthly mean predictability for the 500 hPa height using model as well as observational data for verification. In section 4, the relationship between initial condition memory, atmospheric persistence, and major modes of variability is established. A summary and discussion is provided in section 5.

2. Experiments and analysis procedure

This study is based on four types of predictability experiments, which were conducted with the NCEP seasonal forecasting model (SFM) as described by Kanamitsu et al. (2002) and by RR. The horizontal resolution was T42 (ca. 280 km), and the vertical grid had 28 layers ranging from 995 to 2.7 hPa (assuming 1000 hPa at sea level). Table 1 provides detailed specifications of the experiments, which were carried out in a 10-20

member ensemble mode. Individual forecasts of one experiment were forced with identically evolving boundary conditions, but were started from slightly different initial conditions. They were derived from continuous AMIP-type base runs or NCEP/NCAR reanalysis using the breeding technique (e.g. Toth and Kalnay, 1993). Details about the implementation of the breeding method can be found in RR. Run BASE-O (base run, observed SSTs) was forced with observed global SSTs and sea ice, and run BASE-C (base run, climatological SSTs) was forced with climatological SSTs and sea ice.

The experiments were carried out for 22 years (1979 to 2000). They were started at December (June) 15th and run for 14 weeks until the end of March (September). These periods will be referred to as (northern hemispheric) winter and summer seasons. In all of the simulations, the ozone distribution was prescribed by its zonal mean climatological annual cycle. Each experiment is denoted by a specific acronym in order to indicate the type of initial (ICs) and boundary conditions (BCs). The perfect experiment ICBC was forced with observed global SSTs and sea ice, and model generated land boundary conditions. ICBC was initialized from the base run which was forced with observed ocean boundary conditions (BASE-O). This was equivalent to using "observed" initial conditions, but under a perfect model assumption. . The boundary conditions for experiment iBC were identical to ICBC. The only difference were the initial conditions, which were produced by integrating the forecasts of ICBC for one whole year, i.e. from Dec. 15th to Dec. 15th of the following year. For example, to initialize iBC for 1989, we would run ICBC from 1988 to 1989. These initial conditions were fully adjusted to the boundary forcing, but after one year they had presumably lost almost their entire memory of the previous year. It can therefore be expected that the initial conditions of ICBC and

iBC have a similar large scale structure, but completely different synoptic and smaller scale features. The motivation for this experiment was to find out how much predictability might be lost by excluding the beneficial effects of initial conditions on synoptic and larger scales. The third experiment, IC, used the same initial conditions as ICBC, but was forced with climatological ocean and land boundary conditions derived from NCEP/NCAR reanalysis-2. We repeated ICBC and IC for the winter season with initial conditions obtained from reanalysis and named these experiments IC-r and ICBC-r, respectively. Finally, experiment BC was started from "climatological" initial conditions, but forced with the same perfect boundary conditions as ICBC. These initial conditions were derived from BASE-C for the same date but from randomly selected years.

When interpreting the results from this experimental setup one has to keep in mind several limitations. First, prescribed ocean boundary conditions are used. This assumes that the evolution of ocean boundary conditions is perfectly known at the time of the forecast. In a real forecast situation, however, SSTs are not known a priori. SSTs must be predicted with some statistical or dynamical ocean model, which introduces additional uncertainty into the atmospheric forecast. Therefore, this study investigates the hypothetical upper limit of predictability, which will be referred to from now on simply by predictability. The one-way coupling of the ocean to the atmosphere by prescribing the SSTs can lead to further complications, since in nature air-sea fluxes can go in either direction. While it is believed that in the tropics the ocean is primarily (but not exclusively) driving the atmosphere, the predominant opinion is that in most places outside the tropics the atmosphere drives the ocean. Prescribing extratropical SSTs to the model can therefore lead to unphysical forcing, which is likely to bias our estimate of perfect model

predictability in a positive way. Land surface boundary conditions, on the other hand, are being forecast by the model of this study. It is unclear how realistic and important the added memory from these conditions are for our estimates of long-range predictability. Other "boundary" conditions, which are simply prescribed as constant to the model, but which may actually not perfectly known in a real forecast, and which in nature may change during a forecast, are (1) the chemical composition of the atmosphere (e.g. radiative forcing by ozone), (2) the aerosol load of the atmosphere, and (3) the amount of incoming solar radiation. Finally, one should also keep in mind that our predictability estimates are model dependent, since the real atmosphere as well as other models may show different sensitivities to initial and boundary conditions. Spatial maps of predictability were constructed by calculating at each grid point the temporal anomaly correlation (*AC*) between the time series of a *verification* and a *prediction* data set. To make differences between *AC* values more normal distributed, we applied a Fisher z-transformation (e.g., Roads, 1988) to the correlations before taking differences, i.e.

$$z_i = \frac{1}{2} \ln \frac{(1 + AC_i)}{(1 - AC_i)} \tag{1}$$

and then again transformed back the results. The time series consisted of seasonal or monthly mean fields over 22 years (1979-2000) of the same lag. Anomalies for each experiment were taken with respect to the individual 1979-2000 climatology. Prediction data were 10-member ensemble means of the experiment under consideration, and verification data were single members of the perfect experiment ICBC. Since each member of the verification ensemble could represent real observations, a more robust estimate of the skill was obtained by computing the skill with each member of the ensemble being treated as verification in turn and averaging over the individual results. Some experiments

were also verified against observed atmospheric states obtained from NCEP/NCAR reanalysis.

3. Horizontal structure of predictability

In this section we present maps of monthly mean predictability at the 500 hPa level for different experiments, seasons and verification methods. We focused mainly on monthly mean predictability during forecast week 3-6, which corresponds to January and July. At this time range, the high deterministic predictability period at the beginning of a forecast is mostly excluded, although the effects of initial conditions are likely to be still important, and the averaging period is long enough for boundary effects to be detectable. We focused on predictability of the 500 hPa height, since this variable is widely used in this kind of studies. Predictability of other levels will be described in the following section.

a. Perfect world

The geographical distribution of temporal anomaly correlations of January mean 500 hPa heights is presented in Fig. 1 under perfect model assumption, where ensemble means of each experiment were verified against individual simulations of ICBC. Panels on the left are *AC* scores, and panels on the right show differences to experiment ICBC. Simulation ICBC (top) verified against itself is a measure of the upper predictability limit with respect to initial conditions. Model and boundary conditions were both perfect, but initial conditions contained small imperfections because of small initial perturbations of individual forecasts. These initial differences represent observational uncertainties, which led to a divergence of individual forecasts and thus to a decrease in forecast skill over time. Main regions of high predictability were the tropics, the Pacific-North-American (PNA) region (e.g., Wallace and Gutzler, 1981), and the Pacific-South-American (PSA) region.

The PSA region is the southern hemispheric counterpart to the PNA region (e.g., Karoly, 1989). Interestingly, predictability was also enhanced over the Antarctic continent. Independent experiments by Kumar et al. (2003) with the NSIPP model (Bacmeister et al., 2000) confirm the existence of a high predictable region over the Antarctic continent, indicating that this feature was not just a product of our particular model. Experiment iBC (2^{nd} row) had in general lower skill scores than ICBC, and predictability for BC (3^{rd} row) was even lower, showing the beneficial effect of initial conditions on long-term predictability. This was particularly evident over the Southern Hemisphere, but also to some extent over all other areas.

Experiment IC, on the other hand, had over some regions relatively high predictability just from using initial conditions. These were in particular the Southern Hemisphere, but there was also some skill over the PNA region, the PSA region, and the tropics. The latter was surprising since the tropics are usually regarded as being dominated by influences from boundary forcing. When the *AC* values were calculated only from years where ENSO was strong (not shown), then the skill of experiment IC even increased over the PNA and PSA region, but it decreased over the tropics and the Antarctica. When considering only neutral to weak ENSO years (not shown), then the *AC* scores of experiment IC over the PNA region decreased, and those over the tropics became more evenly distributed. During February and March (not shown), the simulation skill of IC dropped to insignificant values for most areas, whereas the patterns of predictability for iBC and BC became increasingly similar to that of ICBC. The only exception was the region over Antarctica, where the initial condition influence was still detectable in March.

During July (Fig. 2), predictability was generally lower than during January. This was probably related to the relative weakness of ENSO during this time. The only exception was the PSA region with higher skill during July than during January. This might be due to seasonal changes in the atmospheric background state, which led to a stronger ENSO response over the PSA region during southern hemisphere winter. The reduction in skill for iBC and BC, and some areas of skill for IC, showed that initial conditions were also important during July. An important difference from January was that the Antarctic region was much less predictable during July.

b. Zonal averages

Zonally averaged *AC*s were calculated to examine better the latitudinal differences in predictability. Since strong boundary effects during ENSO years are likely to override the more subtle initial condition effects, we analyzed the data separately for strong and neutral-to-weak ENSO years. The chosen ENSO years, which include both warm and cold events, are presented in Table 2; neutral-to-weak ENSO years are all the other years.

Fig. 3 shows zonally averaged *AC*s for January (top) and July (bottom). During January, most notably, experiment ICBC showed at most latitudes the highest forecast skill. During neutral-to-weak ENSO years (left panel), there existed large differences in skill over the tropics, with simulation ICBC clearly the best, iBC better than BC, and IC having surprisingly good skill. Over the northern extratropics, overall skill values were low, but again ICBC had the best skill. South of 30ºS, *AC* scores of IC were very close to that of ICBC, whereas iBC and BC had almost no skill. During ENSO (right panel), initial conditions were, as expected, less important. They were most relevant south of 60ºS. Over the tropics and the northern extratropics, the skill scores of ICBC, iBC and BC were very

close, indicating that boundary forcing dominated predictability during those years. The bottom of Fig. 3 shows the zonally averaged *AC*s for July. As for January, experiment ICBC had the highest skill values at most latitudes. The differences between ICBC and iBC/BC indicated that initial conditions had long term effects also in summer. These differences were largest during weak ENSO years (left panel) over the tropics. Over the extratropics, overall skill values were too small to be significant.

To determine whether initial condition were still important on a seasonal time scale, we repeated the above analysis using January, February and March (JFM) seasonal mean 500 hPa heights (not shown). As one might expect from the decaying influence of initial conditions with lead time, the effect of initial conditions was much weaker for seasonal means. Only over the Antarctic continent were initial condition effects important, and over the tropics during weak ENSO years, initial conditions played some role.

c. Seasonality

We also examined experimental differences between zonally averaged *AC*s for the two contrasting seasons (Fig. 4). The difference BC-ICBC (left panel) is a measure of how much skill was lost by having imperfect initial conditions. At all latitudes and during both seasons, the differences were negative, indicating that initial conditions were important. The reduction in skill was for most latitudes around –0.1, with some regional and seasonal differences. One important exception was the Southern Hemisphere during January with initial conditions clearly dominating. There was also a tendency of initial conditions over the Northern Hemisphere to be less important, and over the tropics initial conditions were somewhat more important during January than during July.

The right panel of Fig. 4 shows the difference in *AC* between BC and IC. Both curves are mostly positive, showing that the contribution of boundary forcing to predictability was larger than that of initial conditions. Again, the curves for winter and summer are quite similar. Note that the small latitudinal variations of the curves for the two seasons are mostly out of phase. Arrows in both diagrams indicate two relative maxima at 30-40ºN (January) and 30-40ºS (July), which are accompanied with relative minima during the opposite month. Comparing with Figs. 1 and 2 shows that these latitudes were related to the PNA and PSA regions. It indicates that the predictability of these patterns is dominated by boundary forcing during winter of the respective hemisphere. This was the time when the jets were well developed, and the resulting atmospheric mean state favored a strong teleconnection response from the tropical ENSO region (e.g., Trenberth et al., 1998). During summer, just the opposite was true, and initial conditions were quite important for the predictability of these patterns. This may be related to the long time scale of these modes at times when eddy kinetic energy was small, and the ENSO teleconnection response was weak.

d. Real world

To determine whether the long-term effects of initial conditions on monthly predictability were real or artifact, we replaced ICBC and IC by ICBC-r and IC-r and verified against reanalysis instead of model data. When comparing these results with the perfect model world (Fig. 3) one should keep in mind that additional model errors and higher sampling uncertainty make the statistics less robust. Fig. 5 shows the zonally averaged results for January. During neutral-to-weak ENSO conditions (left panel), initial condition effects were important over the tropics. Over the extratropics, however, skill

values and their differences are too small to be statistically significant. During strong ENSO years (right panel), boundary forcing tended to dominate forecast skill over the tropics and northern extratropics. Over the southern hemisphere, initial conditions were similarly important as in the perfect model world, as was shown by the strong increase in temporal *AC*s of ICBC and IC over the Antarctic continent. In part, this increase may also be related to observed long-term trends in stratospheric ozone and associated circulation anomalies (e.g. Thompson and Solomon, 2002). These anomalies may have entered the model through the reanalysis initial conditions. The simulations of this study, however, were forced with climatological ozone. Therefore, significant predictability effects would require the anomalous circulation to survive against the forcing with climatological ozone. Overall, the main findings from the perfect model still hold when using observational data, although there was the difficulty of having only one verifying realization.

4. Vertical structure of predictability

The previous section was focused on differences in predictability at one level and one lead time interval. Since other levels may show important differences, we investigated the predictability of zonal mean heights for the whole atmospheric column from the surface to the lower stratosphere and for three different lead time intervals. As in the previous section, predictability was measured by the temporal anomaly correlation of monthly mean heights.

a. Perfect world winter

Fig. 6 presents latitude-height cross sections of perfect model predictability during January (week 3-6), February (week 7-10) and March (week 11-14) for the four experiments. The predictability fields for experiment ICBC and IC are correlations,

whereas the fields for iBC and BC show correlation differences to ICBC. We chose this particular format to make the temporal changes in predictability clearer. The black curve shows the approximate location of the tropopause, which was calculated from the thermal tropopause criterion (Reichler et al., 1996) using monthly mean temperatures from ICBC.

During January, experiment ICBC (Fig. 6, top left panel) had positive *AC* scores everywhere, except over the lower Arctic. Predictability was generally higher over the southern than over the northern hemisphere, and it increased from lower to higher levels. Maxima (*AC*>0.9) were found in the tropical troposphere. Further, predictability was large (*AC*>0.7) in the lower stratosphere, especially over the tropics and the southern hemisphere. Predictability over Antarctica had an equivalent barotropic structure with values increasing upwards into the lower stratosphere. The troposphere at 30-40ºN was also well predictable. This represented the vertical signature of the PNA, which can be seen by comparing with Fig. 1. The signature of the less well predictable PSA can be seen at around 40-50ºS. During February and March, *AC* scores for ICBC generally decreased. This was most notable in the lower stratosphere. Some of these monthly changes in predictability might be explained by seasonalities in the strength of boundary forcing and in the atmospheric mean state, but most of them were related to the loss of initial condition memory. This became clear from the full predictability fields of experiment iBC and BC (not shown), which were quite constant during different months.

The results for iBC (2nd row) and BC (3rd row) are shown as differences to ICBC. They exhibited at all lead times lower predictability than ICBC. The differences were strongest during January, and weakened during subsequent months. The loss in skill from not having perfect initial conditions was most noticeable in the lower stratosphere and over

Antarctica, but during January it also affected the tropics and the northern hemisphere. During January, experiment BC had at all levels higher deficits in skill than iBC, owing to the adjustment of BC to observed boundary conditions. During the other two months, the differences in skill became smaller, but the structures were spatially very coherent, indicating that this may be more than noise. It was particularly surprising that these differences were even detectable during March, underlining the fact that synoptic scale differences in initial conditions can impact predictability out to many weeks.

During January, simulation IC (bottom panels) exhibited significant predictability over the southern hemisphere and in the lower stratosphere. The skill of IC over Antarctica was almost identical to that of ICBC. Further areas of significant skill from initial conditions were the PSA region, the lower troposphere over the tropics, and the PNA region. During the other two months, predictability from initial conditions alone dropped to mostly insignificant values. It is interesting that the predictability patterns displayed by iBC and BC were strikingly similar to that of IC at all three lead times. This means that to first-order the loss in skill from not having perfect initial conditions was similar to the skill of just having perfect initial conditions. In other words, long-term effects of initial and boundary conditions on atmospheric predictability are mostly linear. This is plausible, since non-linear effects grow usually fast and their time scale may be too short to be relevant for sub-seasonal forecasts.

Both experiments ICBC and IC had in the lower stratosphere and over Antarctica relatively high predictability. The opposite was true for the iBC and BC, which came from non-perfect initial conditions. This means that the stratosphere and the Antarctic regions respond slowly to external forcing, and that the initial condition memory is very long. The

predictability patterns even suggest that the Antarctic region may be influenced from the stratosphere. This picture is consistent with observational findings (e.g., Thompson et al., 2002; Baldwin and Dunkerton, 2001) that stratospheric anomalies affect tropospheric circulation, and that these anomalies can be used as predictors for tropospheric weather regimes with lead times of several weeks.

b. Perfect world summer

During boreal summer (Fig. 7), the patterns of predictability were more symmetric to the equator than during winter. During July, predictability for ICBC was highest over the tropics and in the stratosphere, and was lowest over Arctic and Antarctic regions. The separation into different well predictable areas as during winter was less pronounced. The vertical signatures of the PNA and PSA patterns can still be seen at around 40ºN and 30ºS, respectively. The decrease in skill for ICBC during August and September was again related to the loss of initial condition memory, as the comparison with experiment iBC shows. Experiments iBC (2^{nd} row) and BC (3^{rd} row) exhibited a stronger loss in predictability than during winter. During July, most of the atmosphere showed sensitivity to initial conditions, but during the later months, only the stratosphere and the region over the Antarctica were affected. Again, the loss for BC was larger than that for iBC. Experiment IC (bottom row) shows that initial condition effects during summer were most important in the stratosphere. The high predictable area for ICBC and IC over Antarctica during winter had no counterpart during summer over the Arctic. The initial condition effect on the PNA region was larger than that on the PSA region, which was opposite to the winter season (see Fig. 6). This finding was consistent with Fig. 4, and confirms that initial conditions were more important for the ENSO teleconnection regions during

summer than during winter of each hemisphere. Note that the patterns of IC were again quite similar to that of iBC.

c. Seasonality

Next, we explore seasonal differences in the magnitude and spatial characteristics of predictability. It is well known that the strength of the tropical ENSO signal peaks during late winter/early spring, but from this alone it is not obvious how the magnitude of predictability between winter and summer compares. Predictability depends not only on the seasonal cycle of ENSO, but also on the atmospheric mean state and the magnitude of atmospheric internal variability. Fig. 8 shows the seasonal differences in *AC* scores for experiment ICBC. Taking the atmosphere as whole, predictability during winter was clearly higher than during summer, which contradicts findings from Kumar et al.(2003). This was in particular true for the tropics and Antarctica, owing to the stronger ENSO signal and the strong initial condition effect during winter. For the midlatitudes, the situation was more complicated, and a strong function of latitude and height. Possible explanations for the apparent contradiction between the two studies are differences in the models and in the methodologies used to estimate predictability. Clearly more research is necessary to resolve this issue.

d. Real world

Fig. 9 shows vertical cross sections of winter zonal mean predictability for experiment ICBC-r and IC-r verified against reanalysis. The patterns were more noisy since only one member was used for verification. Nevertheless, similar conclusions found previously for the perfect model world also hold under the real world verification. During January, experiment ICBC-r showed high predictability in the tropics, in the stratosphere,

and over the Antarctic continent. Predictability patterns for IC-r were similar to ICBC-r except for the tropics. The loss in skill for experiments iBC and BC was similar to that in the perfect model world. Differences in skill to ICBC were particularly large during January, in the stratosphere, and over Antarctica.

5. Predictability, persistence and major modes

In this section we explore in more detail the long-range predictability and the long memory of initial conditions seen in the previous sections. We were particularly interested in determining whether these effects were due to dynamical predictability in the sense that daily height variations were forecasted well, or whether they was rather due to the atmospheric persistence.

a. Persistence of daily heights

We determined persistence from the ratio between the low- and high-frequency variability of daily 500 hPa height anomalies. The low-frequency component (or signal) for a particular year and member was given by the mean anomaly over the T=48 day long period from Dec. 15th to Jan. 31st. The high-frequency part (or noise) was derived from the daily standard deviation around this mean over the same period. The ratio between signal and noise gave the measure of persistence for one member and year, and the average over all years and members was taken as the ensemble measure of persistence.

The result is shown in Fig. 10 (a) for reanalysis, and for experiments ICBC and IC. In the reanalysis, persistence was particularly high over the tropics and over Antarctica. Over Antarctica, the high-frequency variability was particularly small (not shown), which is probably linked to the low baroclinicity and the low wind speeds typical for Antarctica during austral summer. Additional regions of enhanced persistence could be found over the

North Atlantic, Greenland, the North Pacific off the coast of the U.S., and the Arctic. When persistence was calculated from simulation ICBC, very similar patterns emerged (middle panel). Note that the persistence patterns for ICBC were quite similar to the patterns of predictability shown before (Fig. 1), indicating that there exists a close relationship between long-range predictability and atmospheric persistence. Additional insight can be gained by comparing the persistence patterns from ICBC with that from IC (lower panel). Overall, persistence for IC was much smaller than for ICBC, in particular over the tropics and the two ENSO teleconnection regions. This means that persistence and long range predictability over these regions was mainly related to persistent boundary forcing. Over Antarctica, IC shows similarly large persistence as ICBC. This indicates that over this region persistence is related to low-frequency variability within the atmosphere itself, which in turn is linked to the long initial condition memory.

To further verify our results, a second form of persistence measure was derived from the autocorrelation between daily 500 hPa height anomalies. In Fig. 10 (b), the lag L for the autocorrelation to reach 1/e is shown. This measure of persistence provided similar patterns as before. For reanalysis and ICBC, largest values of L (>20 days) can be seen over the tropics. For simulation IC, L was relatively short over the tropics and the North Pacific, and it was long over Antarctica.

b. Relationship to major modes

Atmospheric persistence was also closely related to the major modes of variability. This is demonstrated by Fig. 11, which shows a composite of the leading modes of variability calculated from individual members of experiment ICBC. The modes were derived from monthly 500 hPa height anomalies using Empirical Orthogonal Function

(EOF) analysis. The analysis was carried out separately for the tropics (30N-30S), the northern (90N-20N) and the southern (20S-90S) extratropics. The first three major modes over the north were derived by rotated EOF analysis technique (e.g., von Storch and Zwiers, 1999). These well known modes were the North Atlantic Oscillation (NAO) (Walker and Bliss, 1932), the PNA pattern, and a pattern similar to the Northern Asian pattern (NA) (Barnston and Livezey, 1987). They explained 12.5%, 11.6%, and 11.0% of the total variance, respectively. For the southern hemisphere, unrotated EOF analysis was used, and only the first mode is shown. This is the Antarctic Oscillation (AAO) (Gong and Wang, 1999), which explains 32% of the total variance. The tropical mode was also derived from unrotated EOFs. It represents the Southern Oscillation (SO) (Walker, 1924), which explains 32% of the total variance.

All of the above modes were characterized by enhanced persistence, as can be seen by comparing with the persistence maps for ICBC shown before (e.g., Fig. 10). This relationship was, of course, not a coincidence, since these modes represent large-scale and low-frequency patterns of variability. EOF analysis from simulation IC (not shown) did not reveal the PNA mode. This means that most of the persistence or low-frequency variability associated with the PNA mode was caused by remote SST forcing, which is consistent with IC not exhibiting much persistence over the North Pacific. Simulation IC exhibited a weak SO mode (not shown) as the third tropical EOF mode. It explained only about 10% of the total variance. This mode was again very similar to the patterns of persistence and predictability exhibited by simulation IC over the tropics. The AAO, on the other hand, was a very robust feature. It was found in all simulations, independent of the kind of SST forcing.

c. Antarctic Oscillation

The relationship between initial condition memory, persistence and the AAO mode over Antarctica is now further described. Fig. 12 shows the pattern of the AAO, derived from 500 hPa height fields from January monthly and ensemble means of simulation ICBC. Only the first 10 members of ICBC (=ICBC-A) were used to construct the EOF. The EOF explained almost 60% of the total variance. As pointed out by Thompson and Wallace (2000), the AAO is characterized by an equivalent barotropic, zonally symmetric structure. Very similar patterns in terms of shape and strength emerged if reanalysis or any other experiments were used.

To determine how important initial conditions were for the simulation of the AAO, we projected the reference EOF from ICBC-A on data from the other experiments and examined the resulting time series (left panels of Fig. 13). The year-to-year fluctuations of the original AAO are shown in the top panel. This time series was well reproduced by ICBC-B, which were the other 10 members of simulation ICBC. The good relationship is also indicated by the rather large correlation shown on the right. Remarkably, the time series from simulation IC correlated also quite well with ICBC-A. On the other hand, the time series for iBC and BC correlated less well with ICBC-A, confirming our previous finding that the predictability of the AAO during January was dominated by initial conditions. The relationship between AAO and initial conditions was also determined from reanalysis and simulations ICBC-r, IC-r, iBC and BC (Fig. 13, right panels). The correlations between the time series were now smaller, but a similar relationship as before held in terms of the different sizes of the correlations.

It should be noted that the AAO index time series of reanalysis, ICBC-r and IC-r exhibited a common long-term trend which helped to improve the correlations. Thompson and Solomon (2002) argued that in the real atmosphere this trend was related to photochemical ozone loss in the stratosphere, which would cause circulation changes in the lower stratosphere, and which in turn would propagate down into the troposphere. Our model was forced with climatological ozone, and the trend was only simulated by simulations with good initial conditions. Thus, it is clear that the trend must have entered the simulations through their initial conditions, where it persisted for a long time because of the slow time scales over Antarctica. As seen before, the AAO was very persistent during January. This raised the question as to whether there existed a relationship between strength and persistence and hence predictability of the AAO. Such a relationship would make sense, since a strong mode involves a large exchange of mass between polar and mid-latitudes, which may take long to equilibrate. That this was indeed the case is demonstrated by Fig. 14, which shows for particular years of the 1979-2000 period the relationship between January mean skill over the southern extratropics (20°S-90°S) and the strength of the AAO index. The strength of the AAO was measured by the value of the index time series for ICBC at January 1st. Skill for particular years was determined from the spatial *AC* over the southern extratropics between one experiment and ICBC.

Experiments ICBC and IC showed a good relationship between magnitude of the index and the corresponding forecast skill. The correlation coefficients were 0.53 and 0.75, respectively. Thus, simply from knowing the strength of the AAO at the beginning of a forecast one can predict how skillful a forecast will be. For experiments iBC and BC, this relationship did not hold, since no good initial condition information were provided.

Interestingly, ENSO also had some influence on the polarity of the AAO, presumably through the teleconnection into the PSA region. From the limited number of samples it seems that a positive (negative) AAO phase was more likely during warm (cold) years.

d. Arctic Oscillation

We repeated the above analysis for the northern hemispheric counterpart of the AAO, the so called Arctic Oscillation (AO) (e.g. Thompson and Wallace, 2000). The AO was defined as the leading mode of unrotated EOF analysis of the 1000 hPa height field. As for the AAO, we measured the predictability of the AO by the correlation of the index time series between ICBC-A and the other experiments. During northern winter, all 3 boundary forced experiments (ICBC-B, BC and iBC) showed at any lead time interval high correlations (0.8-0.9) with the reference experiment ICBC-A (all not shown). The skill of experiment IC in forecasting the AO, on the other hand, was 0.4 in January (i.e. week 3-6), and practically zero at longer leads. During northern summer, boundary forcing led to equally high correlations as during winter. The skill of experiment IC from having only good initial conditions increased to more than 0.6 during July (i.e. week 3-6), but it was again zero at longer leads. In summary, boundary forcing dominated predictability of the AO in both seasons and at all lead times. For week 3-6 forecasts, the initial condition effect was modest during January, but it was rather strong during July. This is in line with the previous results describing hemispheric and seasonal differences in the predictability and persistence.

6. Summary and Discussion

We investigated the spatial and temporal structure of long-range (2 weeks to 1 season) predictability and its sensitivity to initial and boundary conditions. Four AGCM

predictability experiments were designed using different types of initial and boundary conditions. Overall, boundary forcing was the dominant source of long-range predictability, in particular over the tropics and over the extratropical teleconnection regions PNA and PSA. Remarkably, initial conditions were also important for long-range predictability, in particular at the week 3-6 forecast range. This could be detected almost everywhere and in both seasons, but it was strongest in January, during weak ENSO years, and over the Indian Ocean, the PSA region, Antarctica, and in the lower stratosphere. We found that good long-range predictability existed over regions of enhanced atmospheric persistence, and that in turn the patterns of atmospheric persistence resembled well major modes of atmospheric variability. This means that most of the long-range predictability seen in this study can be explained by major modes, which are either related to persistent boundary forcing, or to the slow time scale within the atmosphere itself. Initial conditions were also very important for the lower stratosphere, which was presumably related to the small spatial complexity and large persistence of the stratosphere (Perlwitz and Graf, 2001).

There are two caveats to this study. First, the adequacy of reanalysis over Antarctica and for the lower stratosphere is doubtful. There, observations are sparse, and artificialities of the assimilation model may influence the reanalysis. However, geopotential heights are smoothly varying fields, so that good results may be achieved with relatively few observations. This assumption was confirmed by comparing reanalysis with radiosonde data, which showed that reanalysis from 1979 and on are an excellent proxy for real heights over the southern hemisphere (pers. comm. D. Thompson, 2002). Second, it is unclear how well the model performs in the stratosphere. The model was not specifically

designed for this domain, but it has an adequate vertical resolution in the extratropical stratosphere (11 layers above 200 hPa), which should be capable to simulate well stratospheric wave dynamics in this region.

The existence of good long-range predictability over Antarctica during austral summer deserves some extra comments. It was found that this predictability was initial condition produced, which in turn was related to strong atmospheric persistence over this area. Both perfect and real world verification showed similar results, as well as other modeling (e.g. Kumar et al., 2003) and observational studies (e.g., Trenberth, 1985). Therefore, one can be confident that this effect is real. The strong atmospheric persistence over Antarctica was in turn connected to the AAO, the leading mode of low-frequency variability over the southern hemisphere. Only with good initial conditions was the time series of the AAO index well predicted, whereas boundary forcing alone was unable to produce such results. Forecast skill over the southern extratropics was elevated when the AAO was in a strong phase of either sign. This can be useful for predicting the expected forecast skill.

Predictability over Antarctica showed an equivalent barotropic structure with skill increasing upward into the lower stratosphere. This raises the question whether tropospheric and stratospheric circulations are to some extent connected, and whether this may have an effect on predictability. There are interesting parallels between our result and those from other studies. The observational study by Thompson and Wallace (2000), for example, found that during certain “active seasons”, the tropospheric circulation over the southern hemisphere is coupled to the stratosphere, and that anomalies amplify with height upward into the stratosphere. The “active season” is a 6-8 week interval centered in

November, when the polar vortex is in the process of breaking down. This allows for strong interaction between vertically propagating planetary waves with the stratospheric mean flow (e.g., Charney and Drazin, 1961). Another possible explanation comes from recent studies, which have shown evidence for a downward propagation of stratospheric anomalies into the troposphere (e.g. Baldwin and Dunkerton, 2001). At this point, however, it is unclear whether the model of this study was able to simulate this mechanism, and whether this affected predictability over Antarctica. Clearly, more work is needed to achieve clarification.

One might have expected that predictability over the Arctic in July is similar to that over the Antarctic in January. However, this was not the case here. This may have been related to the sharply contrasting land-sea distribution and stationary wave climatologies of the two hemispheres. The circulation over the southern hemisphere is more zonally symmetric, with fewer baroclinic disturbances and less meridional exchange than over the northern hemisphere. Another important difference is that the Arctic is not snow covered during summer, so that convective disturbances can develop. The permanent snow and ice cover over Antarctica, on the other hand, provides very constant boundary conditions with little or no seasonal variations. And lastly, July is not an active season for troposphere-stratosphere coupling over the Arctic.

Acknowledgements: We thank M. Kanamitsu for many useful comments and for his help with the model. We also would like to thank D. Dommenget for his careful review of the original manuscript and for insightful discussions. Funding for this research was provided by a cooperative agreement with NOAA (NA77RJ0435 and NA17R1231). The views expressed herein are those of the authors and do not reflect the views of NOAA. We

thank the Maui High Performance Computing Center (MHPCC) and the San Diego Supercomputing Center (SDSC) for providing resources for some of the experiments. This work is part of the PhD thesis of T. Reichler. Comments by the anonymous reviewers helped to improve the presentation of these results.

References

Bacmeister, J. T., P. J. Pegion, S. D. Schubert, and M. J. Suarez, 2000: An atlas of seasonal means simulated by the NSIPP 1 atmospheric GCM. *NASA Tech Memo No 104606*, **17,** Goddard Space Flight Center, Greenbelt, MD 20771.

Baldwin, M. P. and T. J. Dunkerton, 2001: Stratospheric harbingers of anomalous weather regimes. *Science,* **294,** 581-584.

Barnston, A. G. and R. E. Livezey, 1987: Classification, Seasonality and Persistence of Low-Frequency Atmospheric Circulation Patterns. *Mon Weather Rev*, **115,** 1083-1126.

Charney, J. G. and P. G. Drazin, 1961: Propagation of planetary-scale disturbances from the lower into the upper atmosphere. *J Geophys Res*, **66,** 83-109.

Gong, D. Y. and S. W. Wang, 1999: Definition of Antarctic Oscillation Index. *Geophys Res Lett*, **26,** 459-462.

Kanamitsu, M., et al., 2002: NCEP dynamical seasonal forecast system 2000. *Bull Amer Meteorol Soc,* **83,** 1019-1037.

Karoly, D. J., 1989: Southern Hemisphere Circulation Features Associated With El Nino - Southern Oscillation Events. *J Climate,* **2,** 1239-1252.

Kumar, A., S. Schubert, and M. Suarez, 2003: Variability and predictability of 200-mb seasonal mean heights during summer and winter. *J Geophys Res*, **108**.

Lorenz, E., 1969: The predictability of a flow which possesses many scales of motion. *Tellus,* **21,** 289-307.

Lorenz, E., 1982: Atmospheric predictability experiments with a large numerical model. *Tellus*, **34,** 505-513.

Mason, S. J., L. Goddard, N. E. Graham, E. Yulaeva, L. Q. Sun, and P. A. Arkin, 1999: The IRI seasonal climate prediction system and the 1997/98 El Nino event. *Bull Amer Meteorol Soc*, **80,** 1853-1873.

Perlwitz, J. and H. F. Graf, 2001: The variability of the horizontal circulation in the troposphere and stratosphere - a comparison. *Theor Appl Climatol*, **69,** 149-161.

Reichler, T. and J. O. Roads, 2003: The role of boundary and initial conditions for dynamical seasonal predictability. *Nonlinear Proc Geophys*, **10**.

Reichler, T., M. Dameris, R. Sausen, and D. Nodorp, 1996: A global climatology of the tropopause height based on ECMWF-analyses. Report 57, DLR, Institute of Atmospheric Physics, 23 pp.

Roads, J. O., 1988: Lagged average predictions in a predictability experiment. *J Atmos Sci*, **45,** 147-162.

Roads, J. O., S. C. Chen, and F. Fujioka, 2001: ECPC's weekly to seasonal global forecasts. *Bull Amer Meteorol Soc*, **82,** 639-658.

Thompson, D. W. J. and J. M. Wallace, 2000: Annular modes in the extratropical circulation. Part I: Month-to-month variability. *J Climate*, **13,** 1000-1016.

Thompson, D. W. J. and S. Solomon, 2002: Interpretation of recent Southern Hemisphere climate change. *Science*, **296,** 895-899.

Thompson, D. W. J., M. P. Baldwin, and J. M. Wallace, 2002: Stratospheric connection to Northern Hemisphere wintertime weather: Implications for prediction. *J Climate*, **15,** 1421-1428.

Toth, Z. and E. Kalnay, 1993: Ensemble Forecasting at NMC - the Generation of Perturbations. *Bull Amer Meteorol Soc*, **74,** 2317-2330.

Trenberth, K. E., 1985: Potential predictability of daily geopotential heights over the Southern Hemisphere. *Mon Weather Rev*, **113,** 54-64.

Trenberth, K. E., G. W. Branstator, D. Karoly, A. Kumar, N. C. Lau, and C. Ropelewski, 1998: Progress during TOGA in understanding and modeling global teleconnections associated with tropical sea surface temperatures. *J Geophys Res-Oceans*, **103,** 14291-14324.

von Storch, H. and F. W. Zwiers, 1999: Statistical Analysis in Climate Research. Vol. 12, Cambridge University Press, Cambridge.

Walker, G. T., 1924: World Weather II. *Mem India Meteor Dept*, **24,** 275-332.

Walker, G. T. and E. W. Bliss, 1932: World Weather V. *Mem Roy Meteor Soc*, **4,** 53-84.

Wallace, J. M. and D. S. Gutzler, 1981: Teleconnections in the Geopotential Height Field During the Northern Hemisphere Winter. *Mon Weather Rev*, **109,** 784-812.

Table and Figure Captions

Table 1: Boundary and initial conditions, ensemble size and simulation period for each experiment. 'r-2' means NCEP/DOE reanalysis-2. Winter refers to Dec. 15th – Mar. 31st of the following year, and summer refers to Jun. 15th – Sep 30th. 'rndm.' indicates randomly chosen initial conditions, 'obs.' means observed (i.e. reanalysis-1), 'cont.' indicates continuous base run over all years, and 'clim.' indicates climatological boundary conditions.

Table 2: Classification of strong ENSO years during January and during July.

Fig. 1. Temporal anomaly correlations of January mean 500 hPa heights assuming perfect model. Left panels are *AC* scores, and right panels are Fisher Z transformed differences to ICBC.

Fig. 2. As Fig. 1 but for July.

Fig. 3. Zonally averaged *AC*s from January (top) and July (bottom) mean 500 hPa heights for neutral-to-weak ENSO years (left) and strong ENSO years (right).

Fig. 4. Difference (Fisher Z transformed) of zonally averaged *AC*s from monthly mean 500 hPa heights from all years under perfect model assumption.

Fig. 5. As Fig. 3 but for ICBC-r and IC-r and verification against reanalysis.

Fig. 6. Vertical cross sections of temporal *AC*s of monthly mean zonal mean heights under perfect model assumption. For experiment ICBC (top row) and IC (bottom row), *AC*

values are shown. For iBC (2nd row) and BC (3rd row), differences (Fisher Z transformed) to ICBC are shown. The black line indicates the location of the thermally defined tropopause. Vertical axis is pressure in hPa, and horizontal axis is latitude in degrees.

Fig. 7. As Fig. 6 but for boreal summer.

Fig. 8. Differences in seasonal predictability for ICBC between JFM and JAS.

Fig. 9. As Fig. 6 but for ICBC-r and IC-r and verified against reanalysis.

Fig. 10: (a) Ratio between mean and spread of daily 500 hPa anomaly fields of individual members from Dec. 15th – Jan. 31st. Shown are averages over the 1979-2000 period and over all ensemble members. (b) Lag *L* in days for autocorrelation of daily wintertime 500 hPa height anomalies to reach e^{-1}. A 3x3 moving box average was applied.

Fig. 11. Composite view of the leading modes of variability of monthly mean 500 hPa height anomalies during winter (JFM), derived from experiment ICBC. The first 3 major modes (NAO, PNA, NA) are shown for the Northern Hemisphere, and the first leading mode (AAO and SO) are shown for the Southern Hemisphere and the tropics. Contour levels are ±40 and ±80 meters (±6 and ±10 in the tropics). Negative contour lines are dashed. The corresponding PC time series were normalized.

Fig. 12. Leading EOF (AAO) over the southern extratropics (20°S-90°S) derived from 500 hPa January monthly mean fields of the ensemble mean of the first 10 members of simulation ICBC. The corresponding time series was standardized, so that the pattern represents average anomalies. Units are geopotential meters.

Fig. 13: (left) AAO index time series derived from projecting reference EOF (shown in Fig. 12) from experiment ICBC-A on monthly mean data from the corresponding simulations. Numbers on the right denote correlation between time series of reference and experiment. (right) As (left), but for reference EOF from reanalysis, and for ICBC-r and IC-r instead of ICBC-B and IC.

Fig. 14. Relationship between January mean skill over the southern extratropics (20°S-90°S) and AAO index at January 1st. The corresponding EOF was normalized, so that units of index (abscissa) are in meters. Ordinate denotes mean pattern correlation between ensemble mean of experiment and individual members of ICBC. Numbers in lower left corner denote correlation coefficient between skill and magnitude of index. Squares in red (blue) denote warm (cold) ENSO years.

Table and Figures

Table 1: Boundary and initial conditions, ensemble size and simulation period for each experiment. 'r-2' means NCEP/DOE reanalysis-2. Winter refers to Dec. 15th – Mar. 31st of the following year, and summer refers to Jun. 15th – Sep 30th. 'rndm.' indicates randomly chosen initial conditions, 'obs.' means observed (i.e. reanalysis-1), 'cont.' indicates continuous base run over all years, and 'clim.' indicates climatological boundary conditions.

	boundary conditions		*initial conditions*				
name	*ocean*	*land*	*atmosphere*	*land*	*size*	*period*	*years*
BASE-O	observed	model	obs. 1/1/48	obs. 1/1/48	1	cont.	'48-2000
BASE-C	clim.	model	obs. 1/1/48	obs. 1/1/48	1	cont.	'48-2024
ICBC	observed	model	BASE-O	BASE-O	20 10	winter summer	'79-2000
ICBC-r	observed	r-2	r-2	-	10	winter	'79-2000
IC	clim.	r-2 clim.	BASE-O	-	10 10	winter summer	'79-2000
IC-r	clim.	r-2 clim.	r-2	-	10	winter	'79-2000
BC	observed	model	BASE-C rndm.	BASE-C rndm.	10 10	winter summer	'79-2000
iBC	observed	model	ICBC, 1 yr lag	ICBC, 1 yr lag	10 10	winter summer	'80-2001

Table 2: Classification of strong ENSO years during January and during July.

January	1983, 1985, 1987, 1989, 1992, 1998, 1999, 2000
July	1982, 1987, 1991, 1993, 1994, 1997

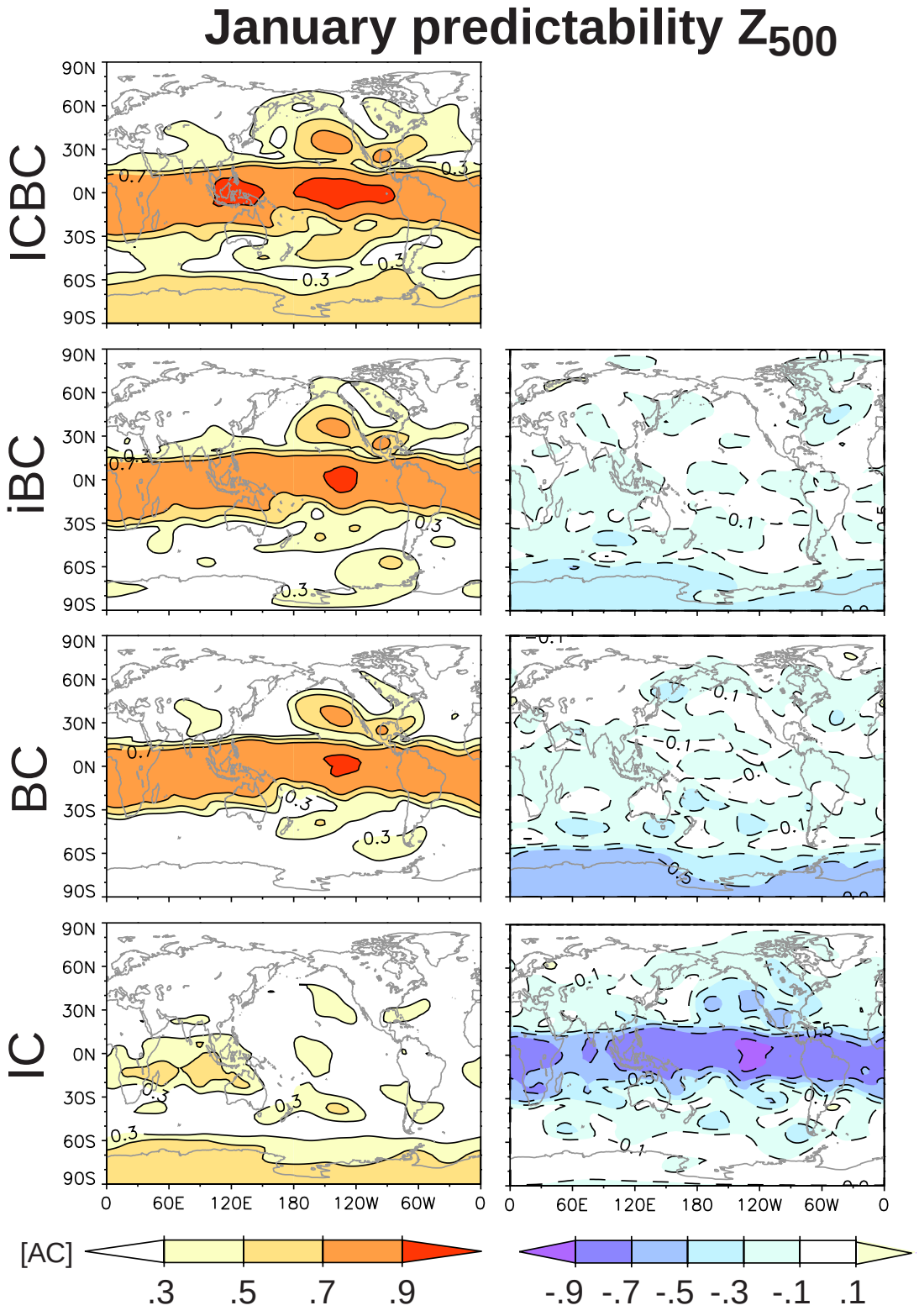

Fig. 1. Temporal anomaly correlations of January mean 500 hPa heights assuming perfect model. Left panels are *AC* scores, and right panels are Fisher Z transformed differences to ICBC.

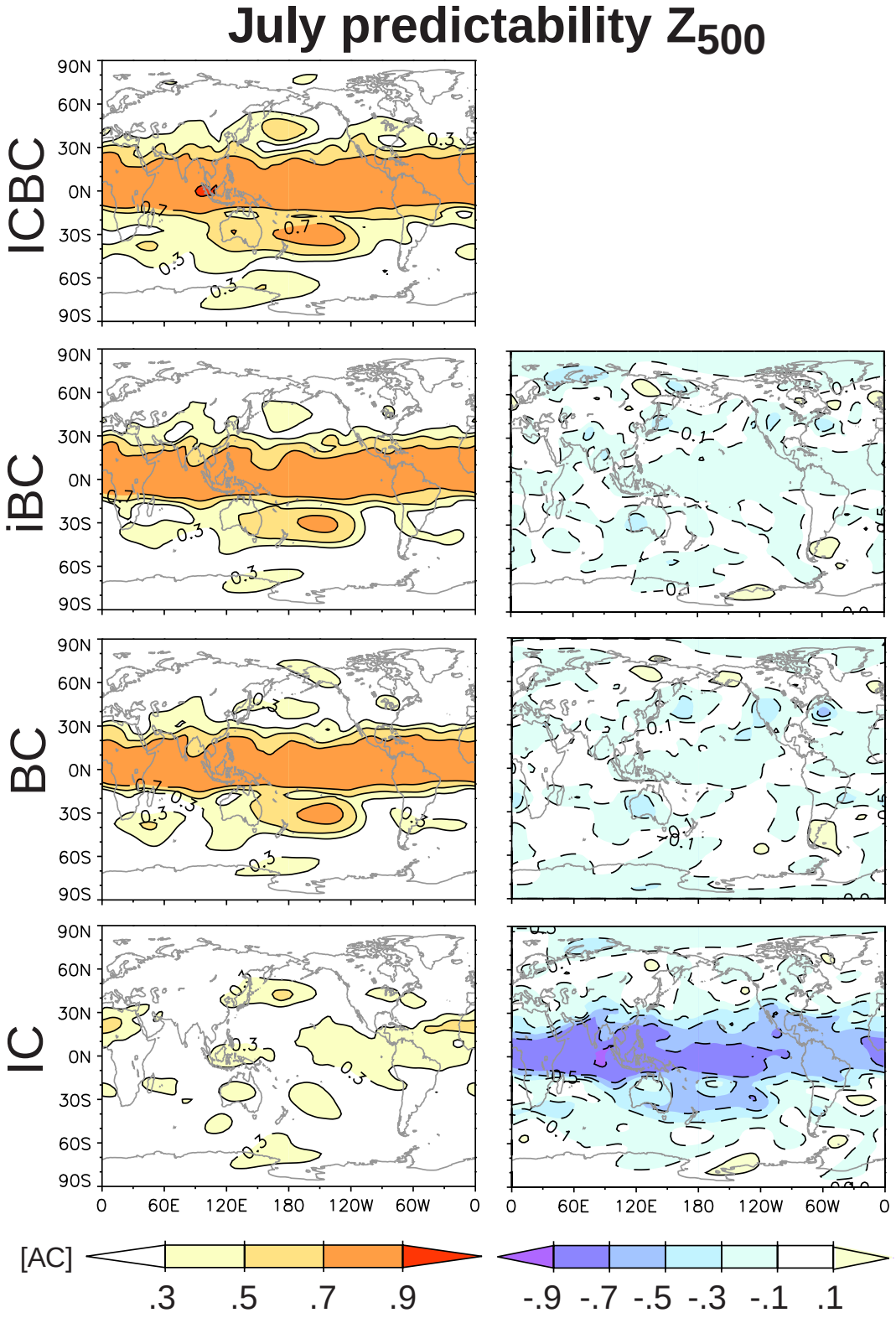

Fig. 2. As Fig. 1 but for July.

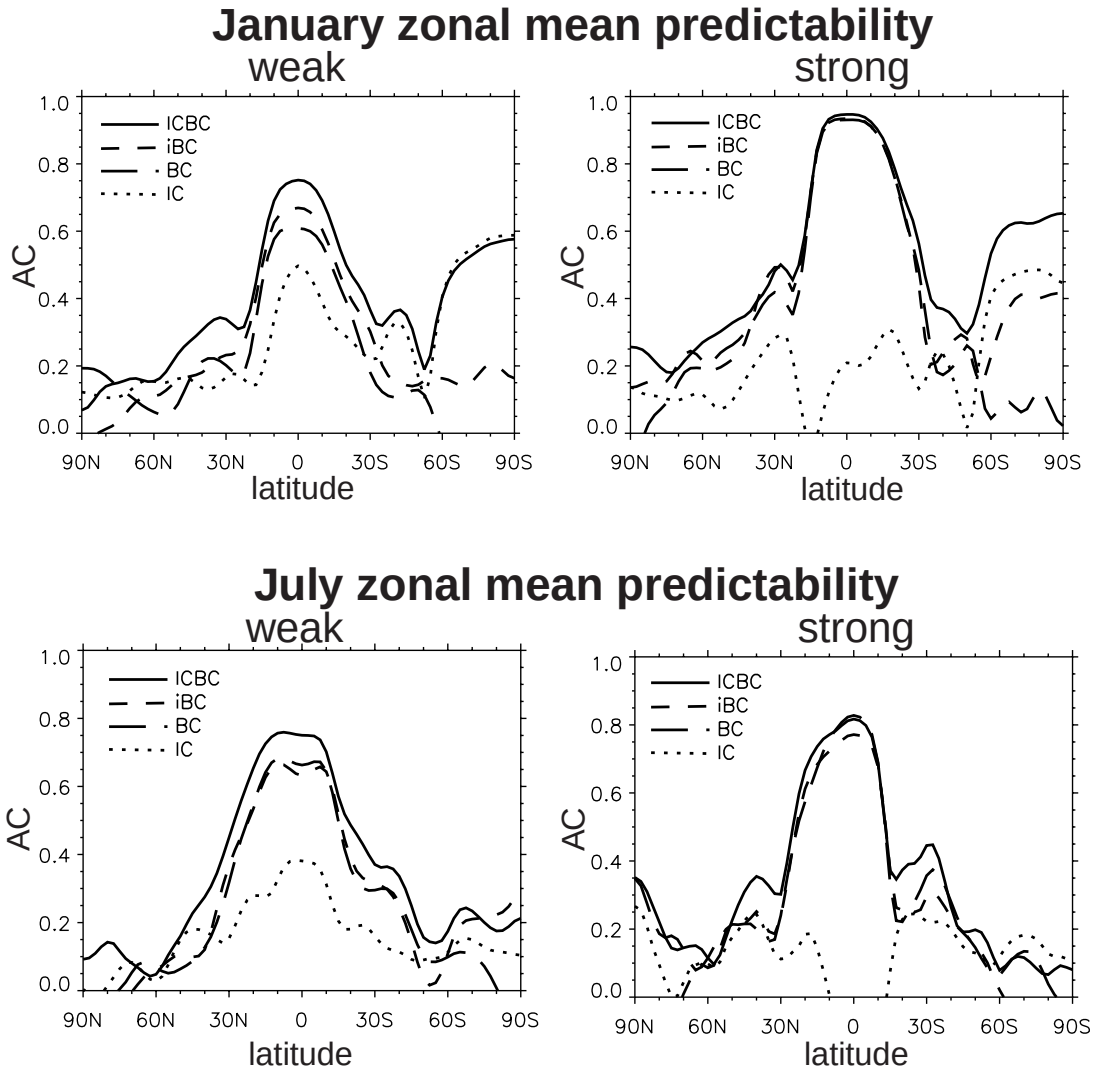

Fig. 3. Zonally averaged *AC*s from January (top) and July (bottom) mean 500 hPa heights for neutral-to-weak ENSO years (left) and strong ENSO years (right).

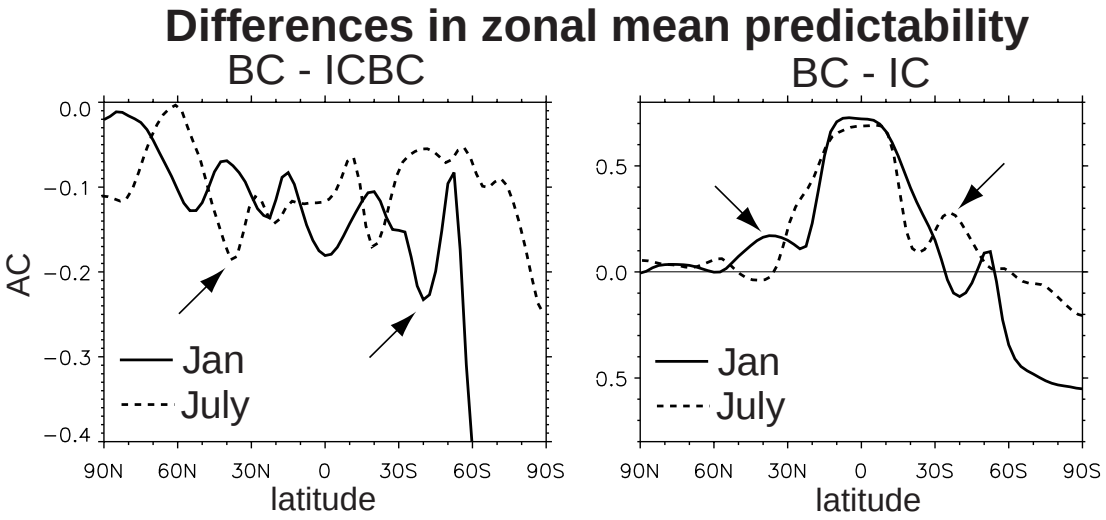

Fig. 4. Difference (Fisher Z transformed) of zonally averaged *AC*s from monthly mean 500 hPa heights from all years under perfect model assumption.

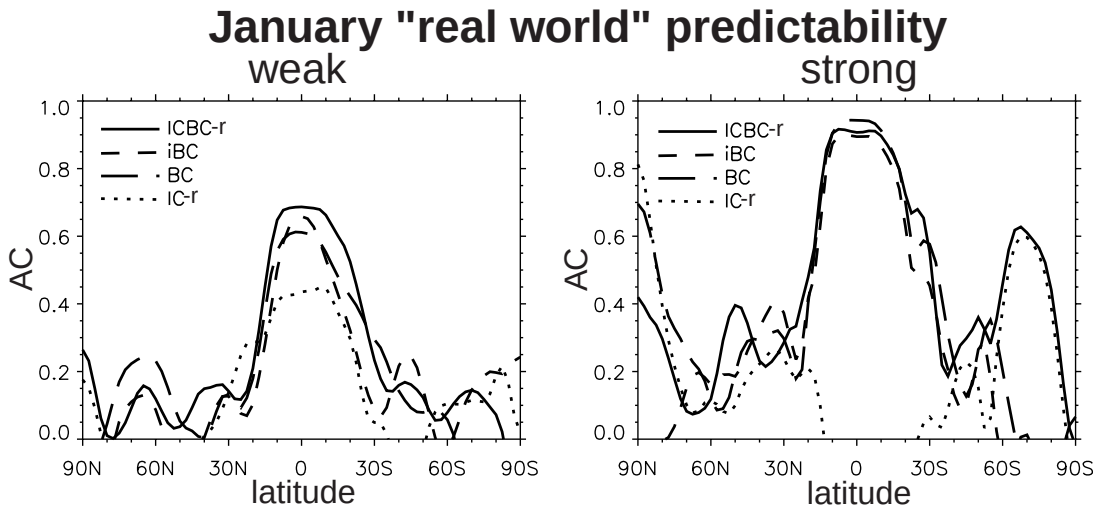

Fig. 5. As Fig. 3 but for ICBC-r and IC-r and verification against reanalysis.

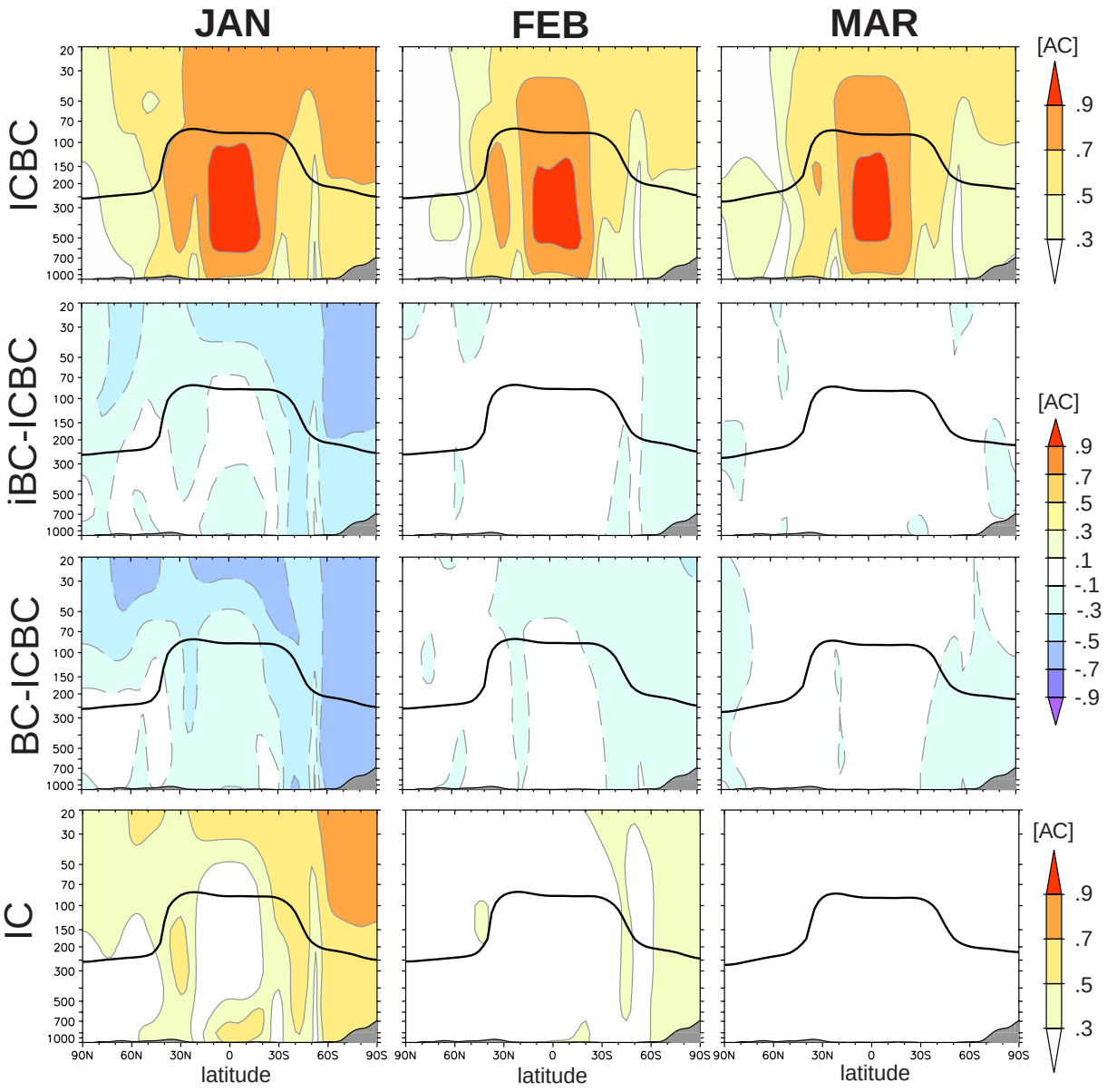

Fig. 6. Vertical cross sections of temporal *AC*s of monthly mean zonal mean heights under perfect model assumption. For experiment ICBC (top row) and IC (bottom row), *AC* values are shown. For iBC (2nd row) and BC (3rd row), differences (Fisher Z transformed) to ICBC are shown. The black line indicates the location of the thermally defined tropopause. Vertical axis is pressure in hPa, and horizontal axis is latitude in degrees.

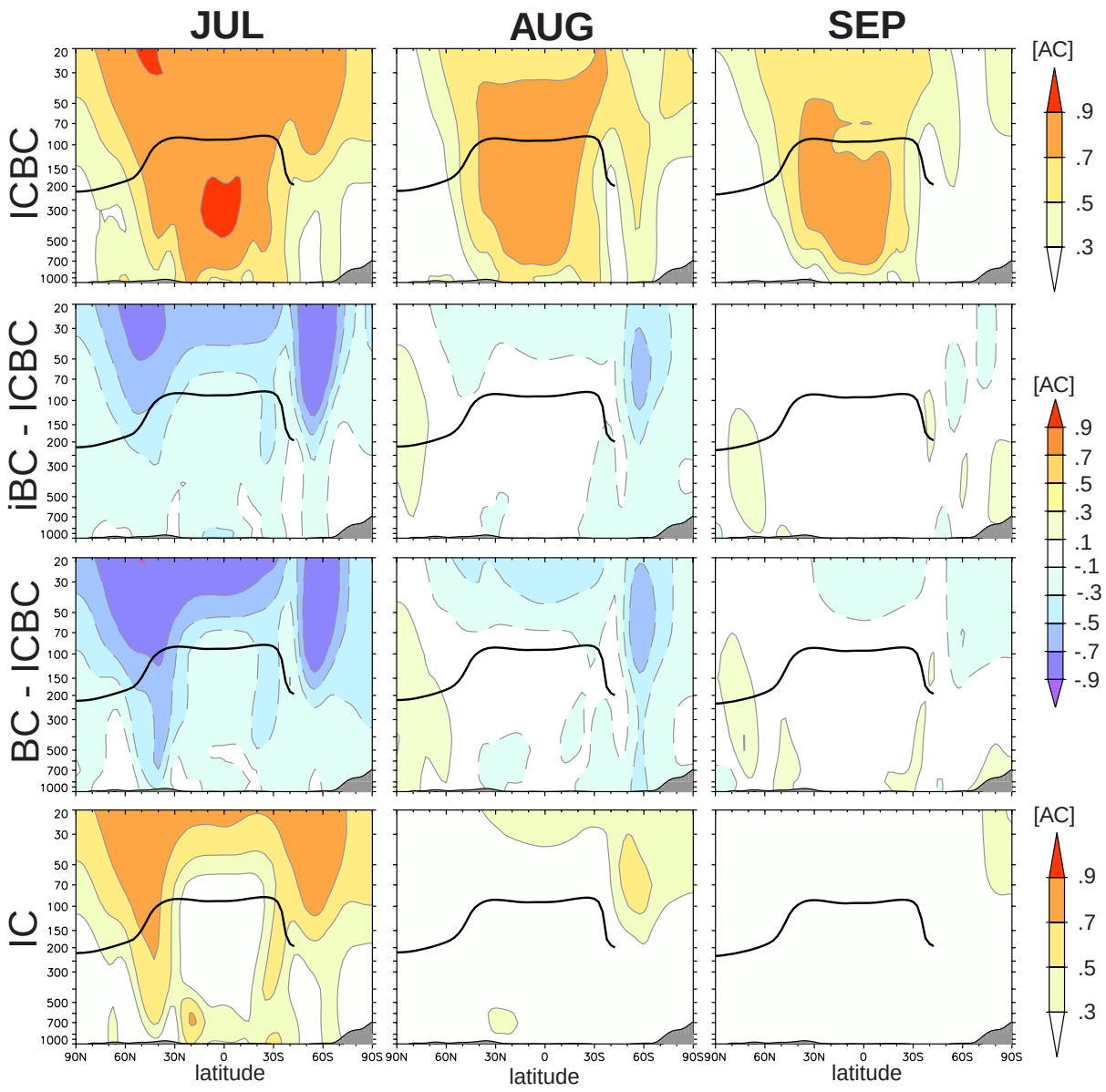

Fig. 7. As Fig. 6 but for boreal summer.

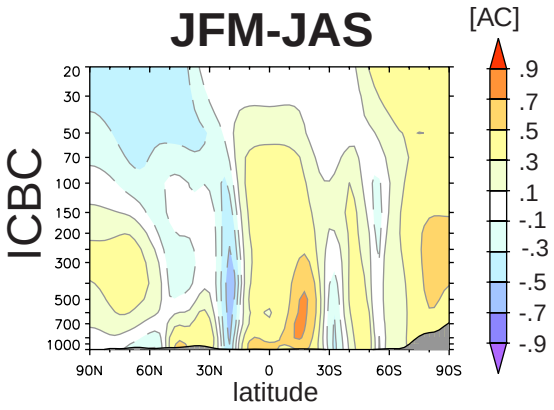

Fig. 8. Differences in seasonal predictability for ICBC between JFM and JAS.

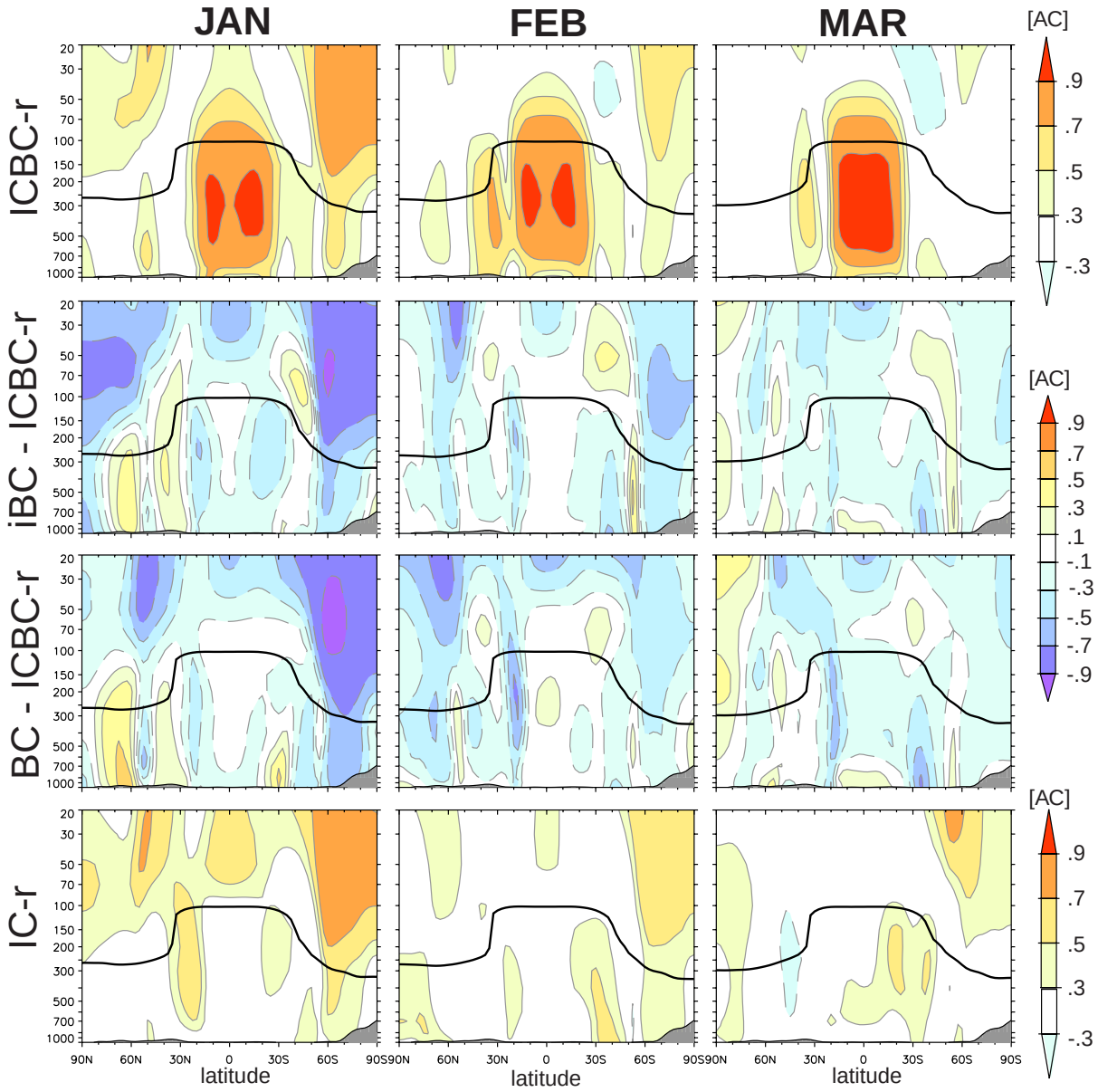

Fig. 9. As Fig. 6 but for ICBC-r and IC-r and verified against reanalysis.

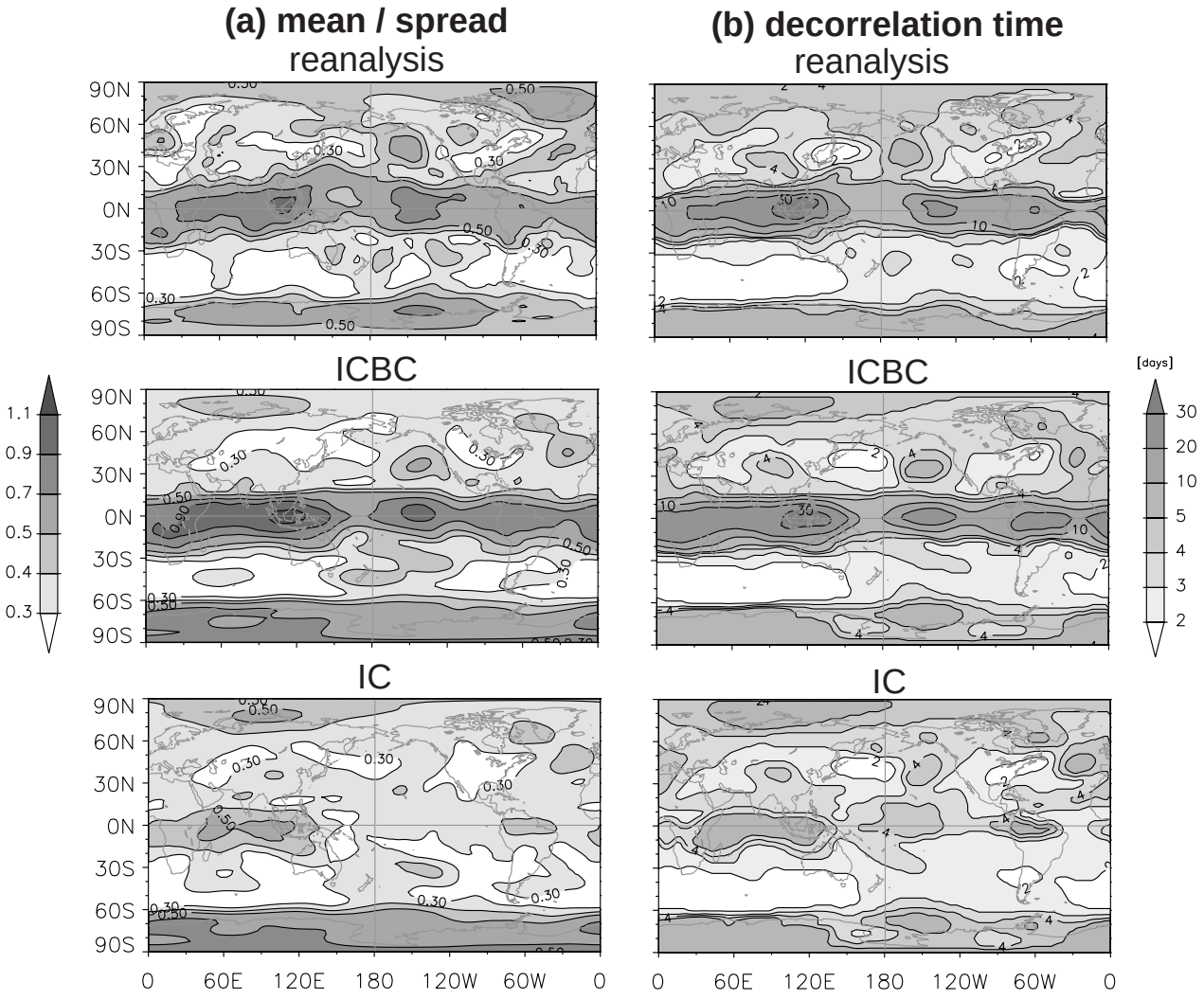

Fig. 10: (a) Ratio between mean and spread of daily 500 hPa anomaly fields of individual members from Dec. 15th – Jan. 31st. Shown are averages over the 1979-2000 period and over all ensemble members. (b) Lag *L* in days for autocorrelation of daily wintertime 500 hPa height anomalies to reach e^{-1}. A 3x3 moving box average was applied.

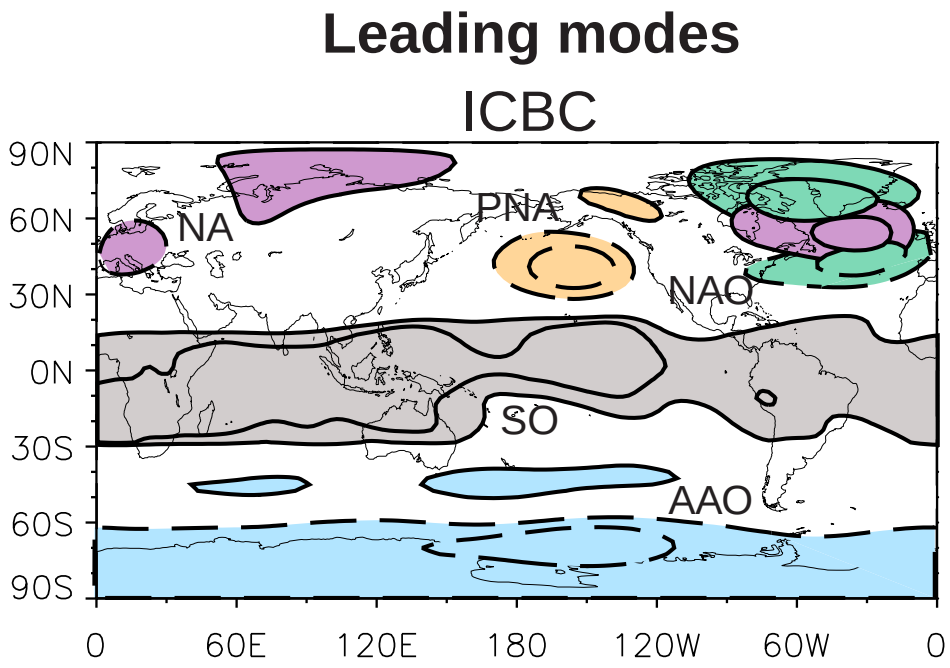

Fig. 11. Composite view of the leading modes of variability of monthly mean 500 hPa height anomalies during winter (JFM), derived from experiment ICBC. The first 3 major modes (NAO, PNA, NA) are shown for the Northern Hemisphere, and the first leading mode (AAO and SO) are shown for the Southern Hemisphere and the tropics. Contour levels are ±40 and ±80 meters (±6 and ±10 in the tropics). Negative contour lines are dashed. The corresponding PC time series were normalized.

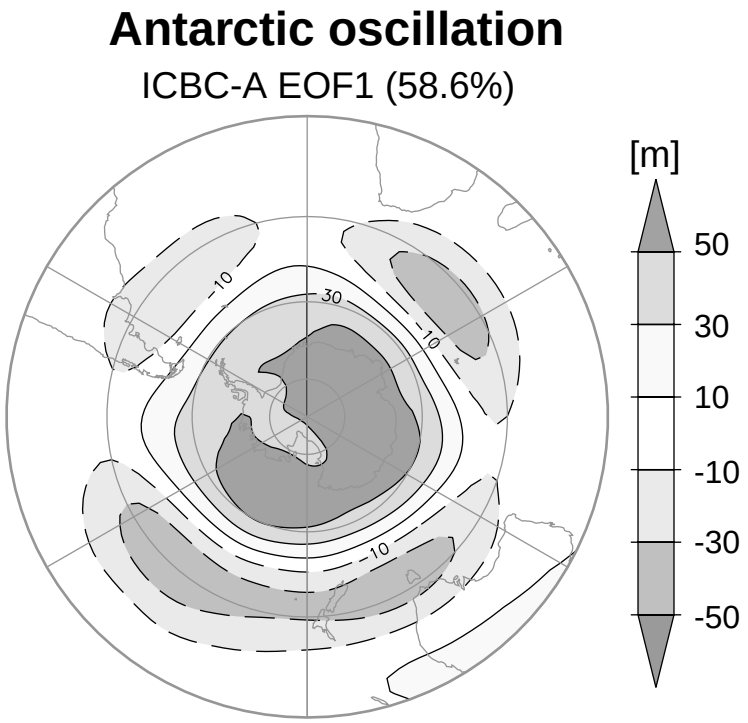

Fig. 12. Leading EOF (AAO) over the southern extratropics (20°S-90°S) derived from 500 hPa January monthly mean fields of the ensemble mean of the first 10 members of simulation ICBC. The corresponding time series was standardized, so that the pattern represents average anomalies. Units are geopotential meters.

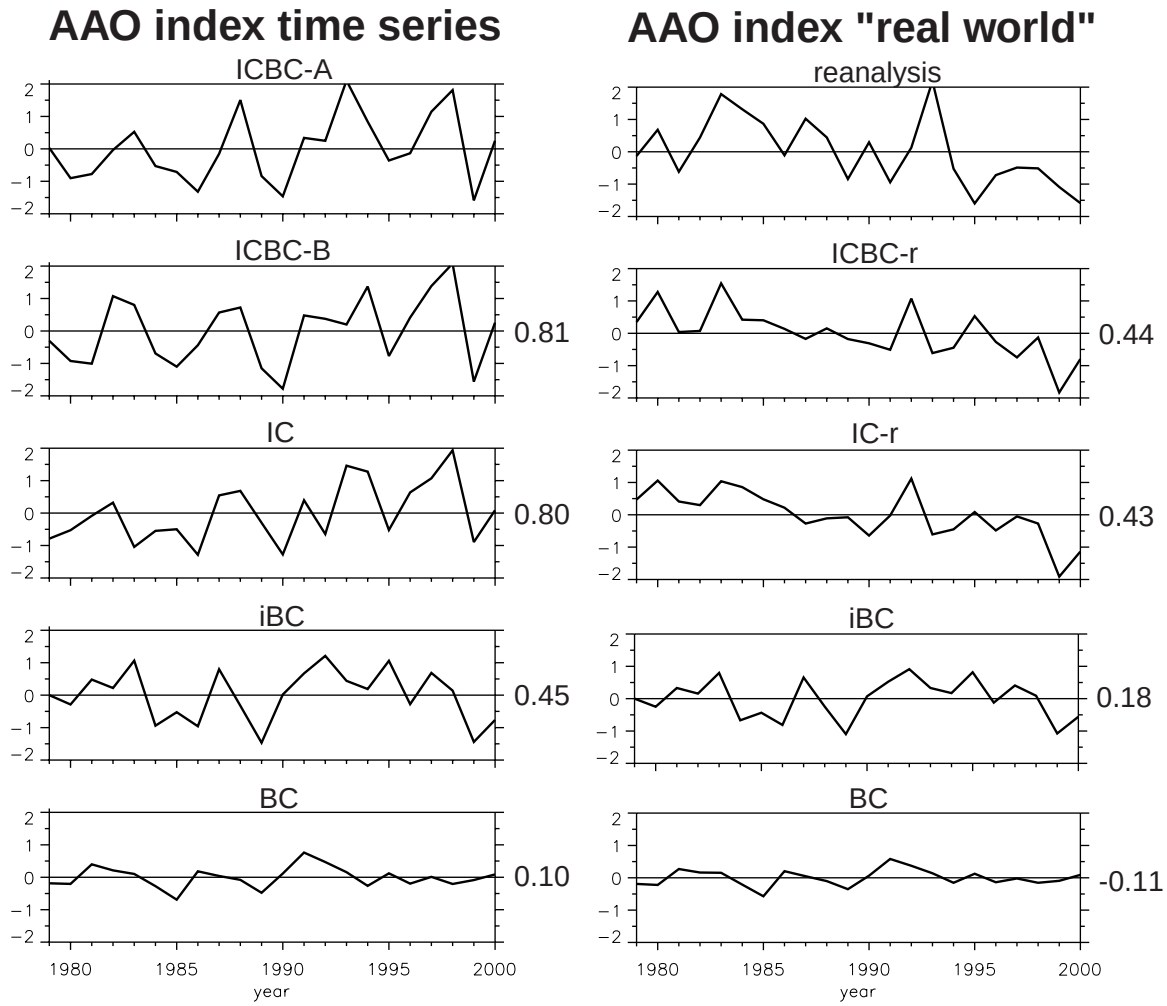

Fig. 13: (left) AAO index time series derived from projecting reference EOF (shown in Fig. 12) from experiment ICBC-A on monthly mean data from the corresponding simulations. Numbers on the right denote correlation between time series of reference and experiment. (right) As (left), but for reference EOF from reanalysis, and for ICBC-r and IC-r instead of ICBC-B and IC.

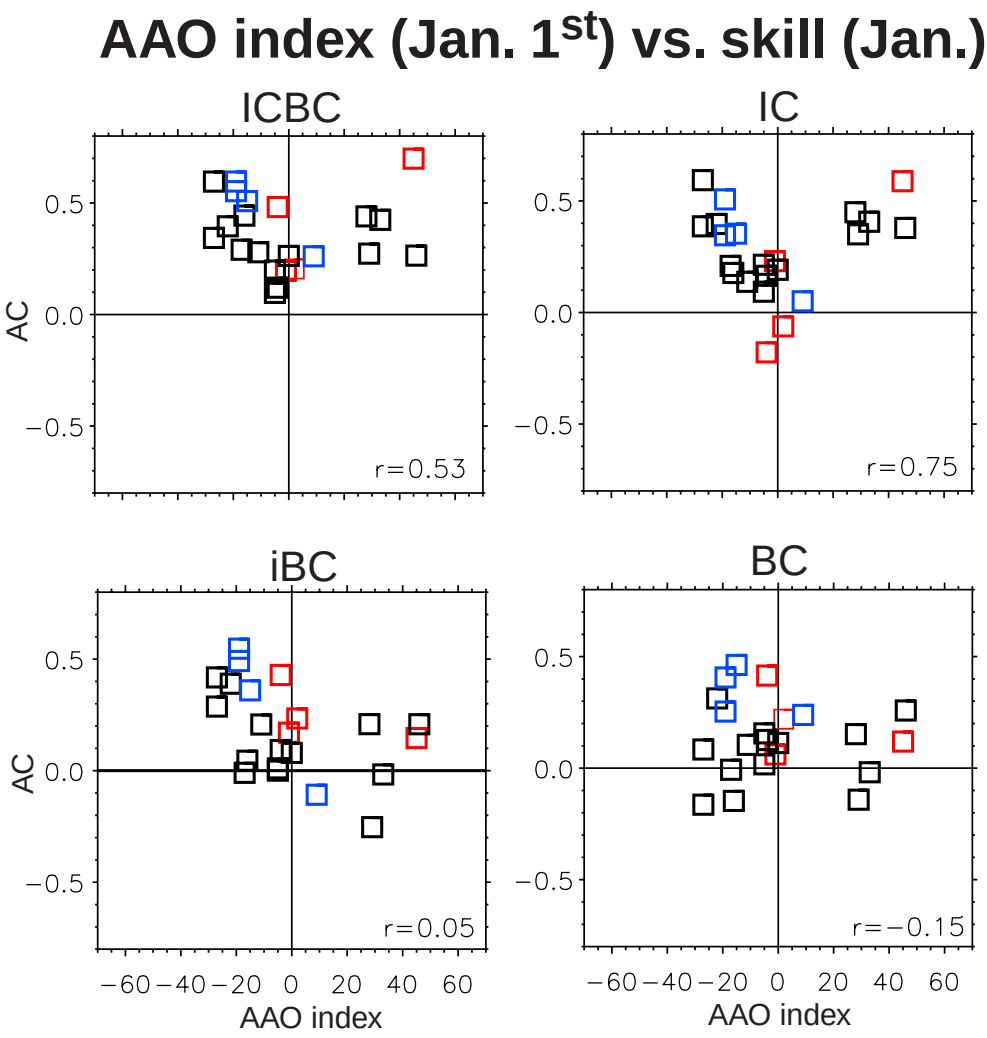

Fig. 14. Relationship between January mean skill over the southern extratropics (20°S-90°S) and AAO index at January 1st. The corresponding EOF was normalized, so that units of index (abscissa) are in meters. Ordinate denotes mean pattern correlation between ensemble mean of experiment and individual members of ICBC. Numbers in lower left corner denote correlation coefficient between skill and magnitude of index. Squares in red (blue) denote warm (cold) ENSO years.